CrossMark

ORIGINAL

R. P. Joseph · B. Wang · B. Samali

Size-dependent stress intensity factors in a gradient elastic double cantilever beam with surface effects

Abstract In this article, the size-dependent stress intensity factors in an elastic double cantilever beam (DCB) are obtained using strain gradient theory. The surface effects are included, while the DCB is assumed to undergo large deformation. Both cracked and uncracked parts (root effect) of the DCB are incorporated in modeling and analyses. The Variational principle is employed to obtain the governing equation and the corresponding boundary conditions. The deflections along the beam axis and stress intensity factors are obtained and plotted. Results exhibit large deformation to be influential for slender beams at small scale. Strain gradient effect tends to increase beam stiffness though reverse holds true for the root effect of the DCB. These effects on structure stiffness are conspicuous when the beam thickness is less than the material characteristic length. Due to positive surface residual stress, beam exhibits less stiff behavior in comparison with the negative surface residual stress. This softening behavior may be credited to the sign of curvature that causes an additional distributed load and alters beam stiffness. It is shown that even with the root effect, negative surface residual stress causes the DCB to display stiffer response by lowering the stress intensity factors and vice versa.

Keywords Stress intensity factors · Double cantilever beam · Strain gradient theory · Surface effects

1 Introduction

Redesigned mixed mode bending (MMB) apparatus, based on geometrical nonlinearity, reduces the error from 30 to 3% in determining its bending behavior [1,2]. The cantilever beam is one of the essential building blocks used in micro and nanoelectromechanical (MEMS and NEMS) devices and often undergoes geometrical nonlinearity. Generally, the geometrical nonlinearity associated with cantilever beam is due to the nonlinear curvature, effect of which is highly substantial [3] (due to the insignificance of Von Karman strain [4,5]). The DCB specimen is widely used to determine the critical stress intensity factors (or strain energy release rate) of homogenous, as well as non-homogenous materials under mode I loading configuration. Furthermore, a double cantilever beam is generally analyzed by examining the bending behavior of a cantilever beam [6,7], since it is considered to be made of two cantilevers attached with an uncracked part. Moreover, the consideration of geometric nonlinearity in the mode I fracture toughness of non-homogenous materials is sufficed for long cracks as shown by Devitt et al. [8] and Williams [9].

Contrary to the classical continuum elasticity theories, the non-classical theories assume that stress at a material point is not entirely depended on the strain at that point but also on all other points in the body [10,11]. This process in literature is referred as the strain gradient effect, and it is more evident when the external and the internal dimensions of the structure become comparable such as in micro-electromechanical

R. P. Joseph · B. Wang (✉) · B. Samali
Centre for Infrastructure Engineering, School of Computing, Engineering and Mathematics, Western Sydney University, Penrith, NSW 2751, Australia
E-mail: b.wang@westernsydney.edu.au

systems (MEMS) and nanoelectromechanical systems (NEMS). In that case, microstructural length scales of a particular material become comparable to the length scale of the deformation field that eventually leads to a non-homogenous and size-dependent structural behavior [6]. The strain gradient model employed in this work was introduced by Aifantis [12], Ru and Aifantis [13], and Vardoulakis & Sulem [14], which is considered more convenient in applications [6,15]. The Cauchy stress (τ_{xx}) and double stress (μ_{xxx}) for the 1-D case are given as: $\tau_{xx} = E\varepsilon_{xx}$ and $\mu_{xxx} = l^2 E \frac{d\varepsilon_{xx}}{dx}$ respectively [7]. Here, E is Young's Modulus; ε_{xx} is the axial strain in the beam due to bending, l is the material microstructural length constants related to the bulk strain energy. The total stresses (σ_{xx}) for the beam bending can be evaluated as: $\sigma_{xx} = \tau_{xx} - \frac{d\mu_{xxx}}{dx} = E(\varepsilon_{xx} - l^2 \frac{d^2\varepsilon_{xx}}{dx^2})$. The application and validation of this simpler strain gradient theory are presented by Vardoulakis & Sulem [14] and Giannakopoulos et al. [6], respectively. A comprehensive review of this gradient theory along with the applications of internal length gradient across various scales is provided by Aifantis [16,17].

There are certain molecular effects that are fascinatingly obvious when the structural dimensions are in micro and nanometer range. Effect of the surface stresses is one of those effects that have thoroughly been explained [18,19]. The atoms on or near the free surface have different equilibrium requirements as compared to the ones in bulk. This difference causes an excess energy at the surface which is understood as a layer to which that energy is attached [20]. Accordingly, the thermodynamic theory of solid surface revealed that the relationship between the surface stress and surface free energy is obtainable [21–24]. Meanwhile, when the size of the structure is reduced to micro/nanoscale, the ratio of the surface area to bulk volume may become enormous. Therefore, the influence of surface effect on the mechanical behavior of the micro/nanomaterials becomes prominent and hence cannot be neglected [25]. Surface effects on micro/nanostructures may be characterized by two major types, i.e., the surface elasticity and the surface residual stress [26]. Gurtin and Murdoch [27] firstly considered the effect of surface stress in their theoretical framework based on continuum elasticity. In their work, the surface is considered as a mathematical layer of zero thickness with different material properties as compared to an underlying bulk. This theory has shown an excellent capability to successfully cater the surface effect on the mechanical behavior of the micro/nanostructures and is widely employed by the researchers throughout [28–33]. The general expression for the surface stress–strain relation is given as: $\sigma^s_{\alpha\beta} = \tau_0\delta_{\alpha\beta} + (\tau_0 + \lambda^s)\varepsilon_{yy}\delta_{\alpha\beta} + 2(\mu^s - \tau^s)\varepsilon_{\alpha\beta} + \tau_0 u^s_{\alpha,\beta}$, where λ^s and μ^s are the surface Lame constants, δ is Kronecker delta, and τ_0 is the surface residual stress in the unconstrained condition. In general, the surface properties usually have anisotropic stress [34–36] depending upon the crystallographic direction of the surface. However, it is shown in the literature that a surface may assume anisotropic nature and it is still meaningful to use an appropriate average of the surface stresses [37–39].

The surface elastic model is effectively employed by the researchers with both surface residual stress and surface elasticity effects in the continuum model [34,40]. Moreover, the surface elastic model along with the generalized Young-Laplace equation has also been widely used to investigate the influence of surface effects on the mechanical response of nanostructures such as nanobeams/wires [26,41,42], nanoplates [43–45] and electrostatically actuated nanobeams [46–49]. However, the contribution of surface residual stress to the total surface stresses is considerably more noticeable than the surface elasticity [33,50]. As mentioned before that the DCB is a widely used specimen for the determination of fracture toughness of a particular material. However, very few efforts have been devoted to study its fracture behavior with the consideration of surface effect [25]. For precise fracture analysis, the future application of micro/nanomaterials demands an inclusion of surface effects in the crack tip field quantities such as strain energy release rate or stress intensity factor. This paper establishes the numerical analysis of a DCB specimen, subjected to large deformation, for the characterization of micro/nanomaterials, with the simultaneous consideration of surface effects and strain gradients. The schematic diagram of a DCB with surface residual stress is shown in Fig. 1a. Size-dependent fracture analysis of a DCB in terms of stress intensity factors with various beam configurations is presented. Finally, the role of uncracked part of the DCB (root effect) is elaborated to conclude this study.

2 Theoretical formulations of the size-dependent bending of a cantilever beam

Classical beam theory is inadequate to correctly evaluate the solution of a cantilever beam under large deformation (at enhanced loads in particular), primarily as it ignores the shortening of moment arm as the free end of the beam deflects. Due to this reason, the classical results deviate from the actual observations at elevated loads. The correction for this shortening of moment arm plays a key role in solving large deformation problems. For one dimension structure, the stress–strain relation for the bulk material (in case of large deformation) is
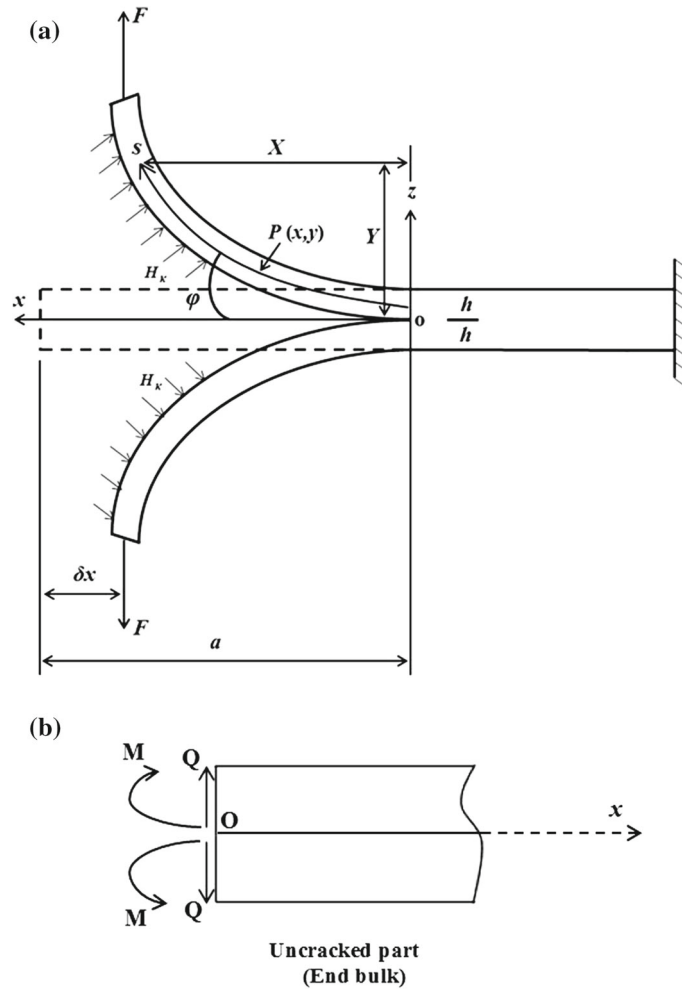
Fig. 1 Schematic diagram of **a** a double cantilever beam with surface residual stress; **b** the uncracked part

given as: $Ez\dfrac{\mathrm{d}\varphi}{\mathrm{d}s} = \sigma_{xx}$, where φ is the slope of beam and E is the Young's Modulus. For surface layer, the stress (τ^s) can be expressed as [51];

$$\tau^s = \tau_o + E_s\varepsilon^s_{xx} \tag{1}$$

where τ_o is the surface residual stress, E_s and ε^s_{xx} are Young's modulus and surface strain, respectively. Accordingly, the bending moment of a beam is given as:

$$M = \int_b z\sigma_{xx}\mathrm{d}A + \int_C E_s\varepsilon^s_{xx}\mathrm{d}C = EI_{\text{eff}}\frac{\mathrm{d}\varphi}{\mathrm{d}s} \tag{2}$$

where C is the perimeter of the beam's cross-section, $EI_{\text{eff}} = \frac{Ebh^3}{12} + \frac{E_sh^3}{6} + \frac{E_sbh^2}{2}$ [26,42]. At any specified point $P(x, y)$ along a curved beam, moment is given as: $M = F.(a - \delta x - x)$ (where a is the length of a beam and δx is the horizontal deflection), which if differentiated $(\mathrm{d}(a - \delta x - x)/\mathrm{d}s = -\cos\varphi)$ gives;

$$EI_{\text{eff}}\frac{\mathrm{d}^2\varphi}{\mathrm{d}s^2} + F\cos\varphi = 0 \tag{3}$$

Vertical deflection Y and arc length s (along with the beam axis) may be evaluated as:

$$s = \sqrt{\frac{EI_{\text{eff}}}{2F}}\int_0^\varphi \frac{\mathrm{d}\varphi}{\sqrt{\sin\varphi_o - \sin\varphi}} \tag{4}$$

$$\frac{Y}{a} = \frac{1}{\sqrt{2}\alpha} \int\limits_0^{\varphi_o} \frac{\sin\varphi \, d\varphi}{\sqrt{\sin\varphi_o - \sin\varphi}}; \text{ here } \alpha = \sqrt{\frac{Fa^2}{EI_{\text{eff}}}} \text{ and } a = \text{length of the beam} \qquad (5)$$

Here, φ_o depicts an unknown slope at the free end. Eqs. (4) and (5) are usually solved numerically to evaluate Y. Alternatively, numerical techniques are applied to Eq. (3) to get φ and deflection Y by the following relation;

$$Y = \int\limits_0^a \sin(\varphi) \, ds \qquad (6)$$

These straightforward formulations may not be precisely applied at micro/nanoscale due to the predominant size effect. In order to cater this, several strain gradient theories are available in the literature (mostly dealing with second-order strain gradients). The constitutive equation for the one-dimensional case in combination with the linear elastic material behavior is written as [15,52,53];

$$\sigma = E(\varepsilon - l^2 \nabla^2 \varepsilon) \qquad (7)$$

where σ and ε are the axial stress and strain respectively, E is Young's modulus, l is the material characteristic length and $\nabla^2 = \partial^2/\partial x^2 + \partial^2/\partial y^2 + \partial^2/\partial z^2$ is the Laplacian operator. Strain for the Euler–Bernoulli beam is given as: $\varepsilon = z\kappa = z\frac{d\varphi}{ds}$, where κ is the curvature and φ is the deformed angle. The ∇^2 operator is reduced to cater only 1D gradient since the deformation is entirely the function of "s" (although a beam is defined in 2D geometrical space, i.e., xy-plane). For 1D cantilever beam, i.e., $\sigma_{yy} = \sigma_{zz} = \sigma_{yz} = \sigma_{xz} = \sigma_{xy} = 0$ (the beam length should at least 10 times of its height [54]), according to Eq. (7), the total stress (σ_{xx}) may be written as:

$$\sigma_{xx} = Ez \left[\frac{d\varphi}{ds} - l^2 \frac{d^3\varphi}{ds^3} \right] \qquad (8)$$

Bending moment at x is given as: $M = \int\limits_A \sigma_{xx} z \, dA$. Using Eq. (8) in the bending moment (for the bulk) equation and upon integration over the cross-section area A, one gets:

$$M = EI \left[\frac{d\varphi}{ds} - l^2 \frac{d^3\varphi}{ds^3} \right] \qquad (9)$$

here l is the material characteristics length. Here, $I = \int\limits_A z^2 \, dA$ is the second moment of cross-sectional area. Now, the governing equation and the corresponding boundary conditions of a strain gradient elastic cantilever beam are evaluated through a variational principle given as: $\delta(U_b + U_s) - \delta W = 0$, where W is the work done by the external forces, U_b and U_s are the strain energy of the bulk and surface, respectively. For one-dimensional case, the bulk strain energy U_b may be written as:

$$U_b = \frac{1}{2} \int\limits_A \int\limits_0^a [\tau_{xx}\varepsilon_{xx} + \mu_{xxx}.\nabla\varepsilon_{xx}] \, ds \, dA \qquad (10)$$

where $\tau_{xx} = E\varepsilon_{xx}$ and $\mu_{xxx} = l^2 E(d\varepsilon_{xx}/ds)$ are the Cauchy and double stress, respectively, ε_{xx} is the axial strain and $\nabla\varepsilon_{xx} = d\varepsilon_{xx}/ds$ denotes the strain gradient. Accordingly, Eq. (10) may be written as: $U_b = (EI/2) \int [(d\varphi/ds)^2 + l^2(d^2\varphi/ds^2)^2] ds$, where $I = bh^3/12$ is the moment of inertia. The variation of the integral of the type $U = \int\limits_0^a F(\varphi', \varphi'') ds$ (where $\varphi' = d\varphi/ds$ and $\varphi'' = d^2\varphi/ds^2$) is given as:

$$\delta U = \int\limits_0^a \left[\left\{ -\frac{d}{ds}\left(\frac{\partial F}{\partial \varphi'}\right) + \frac{d^2}{ds^2}\left(\frac{\partial F}{\partial \varphi''}\right) \right\} \delta\varphi \right] ds + \left[\left\{ \left(\frac{\partial F}{\partial \varphi'}\right) - \frac{d}{ds}\left(\frac{\partial F}{\partial \varphi''}\right) \right\} \delta\varphi' \right]_0^a$$

$$+ \left[\left\{ \left(\frac{\partial F}{\partial \varphi''}\right) \right\} \delta\varphi'' \right]_0^a \qquad (11)$$

From Eqs. (10) and (11) one gets:

$$\delta U_b = \int_0^a \left[-EI \left\{ \left(\frac{\partial^2 \varphi}{\partial s^2} - l^2 \frac{\partial^4 \varphi}{\partial s^4} \right) \right\} \delta\varphi \right] \mathrm{d}s + \left[\left\{ EI \left\{ \left(\frac{\partial \varphi}{\partial s} - l^2 \frac{\partial^3 \varphi}{\partial s^3} \right) \right\} \delta\varphi \right\} \delta\varphi' \right]_0^a$$
$$+ \left[EIl^2 \left\{ \frac{\partial^2 \varphi}{\partial s^2} \right\} \delta\varphi'' \right]_0^a \tag{12}$$

Similarly, the surface strain energy is written as:

$$U_s = \frac{1}{2} \int_A [\tau_{xx}^s \varepsilon_{xx}^s + \mu_{xxx}^s . \nabla \varepsilon_{xx}^s + \tau_o \varepsilon_{xx}^s] \mathrm{d}A \tag{13}$$

From Eqs. (11) and (13), one gets:

$$\delta U_s = \int_0^a \left[\left[-EI_s \left\{ \left(\frac{\partial^2 \varphi}{\partial s^2} - l^2 \frac{\partial^4 \varphi}{\partial s^4} \right) \right\} \right] \delta\varphi \right] \mathrm{d}s + \left[\left[EI_s \left\{ \left(\frac{\partial \varphi}{\partial s} - l^2 \frac{\partial^3 \varphi}{\partial s^3} \right) \right\} \right] \delta\varphi' \right]_0^a$$
$$+ \left[\left[EI_s l^2 \left\{ \frac{\partial^2 \varphi}{\partial s^2} \right\} \right] \delta\varphi'' \right]_0^a - \int_0^a T^s \delta\varphi \mathrm{d}s \tag{14}$$

where $I_s = (bh^2/2 + h^3/6)$ and $T^s = \int_0^a q \mathrm{d}s$, with $q(s)$ is the vertical load induced by the residual stress. According to the Young-Laplace equation [34,40], stress jump across each surface depends on the surface curvature that can be expressed as [34,40]; $\langle \sigma_{ij}^+ - \sigma_{ij}^- \rangle n_i n_j = \tau_{\alpha\beta}^s \kappa_{\alpha\beta}$, where n_i denotes the unit vector normal to the surface, σ_{ij}^+ and σ_{ij}^- are, respectively, the stresses above and below the surface, $\kappa_{\alpha\beta}$ is the surface curvature. Therefore, equivalent vertical load $q(x)$ induced by the residual stress is expressed as [26,42];

$$q = H\kappa = H \frac{\mathrm{d}\varphi}{\mathrm{d}s} \tag{15}$$

with $H = 2\tau_o b$ [26,42,55] where b is the width of the beam. The total force along the beam axis "s" is given as: $T^s = \int_0^a H \frac{\partial \varphi}{\partial s} \mathrm{d}s$. The variation of the work done by the external forces is written as: $\delta W = \int_0^a F \cos\varphi(s)\delta\varphi \mathrm{d}s$. So, the variational principle $\delta(U_b + U_s) - \delta W = 0$ gives:

$$\int_0^a \left[\left[-EI_{\mathrm{eff}} \left\{ \left(\frac{\partial^2 \varphi}{\partial s^2} - l^2 \frac{\partial^4 \varphi}{\partial s^4} \right) \right\} + H\varphi - H\varphi_{(a)} - F\cos\varphi \right] \delta\varphi \right] \mathrm{d}s -$$
$$\left[\left[EI_{\mathrm{eff}} \left\{ \left(\frac{\partial \varphi}{\partial s} - l^2 \frac{\partial^3 \varphi}{\partial s^3} \right) \right\} \right] \delta\varphi' \right]_0^a + \left[\left[EI_{\mathrm{eff}} \left\{ \left(\frac{\partial^2 \varphi}{\partial s^2} \right) \right\} \right] \delta\varphi'' \right]_0^a = 0 \tag{16}$$

The governing equation can be written as:

$$EI_{\mathrm{eff}} \left[\frac{\mathrm{d}^2 \varphi}{\mathrm{d}s^2} - l^2 \frac{\mathrm{d}^4 \varphi}{\mathrm{d}s^4} \right] = -F\cos\varphi + H\varphi - H\varphi_{(a)} \tag{17}$$

where $EI_{\mathrm{eff}} = E\frac{bh^3}{12} + E_s(\frac{h^3}{6} + \frac{bh^2}{2})$. It is necessary to mention for simplification that the size dependence of E is not considered, as previously done in these references [56,57]. Our model applies to those materials that do not show the significant dependence of E on size. The boundary conditions evaluated from the variational principle require $EI_{\mathrm{eff}}[(\partial\varphi/\partial s) - l^2(\partial^3\varphi/\partial s^3)]$ (moment) and $EI_{\mathrm{eff}}(\partial^2\varphi/\partial s^2)$ (higher order moment) to be specified at $s = 0$ and $s = a$. So, one of the possible set of boundary conditions considered in this work is as follows; At clamped end, i.e., $s = 0$, slope, i.e., rotation of the beam is zero $\varphi = 0$, and the non-classical

terms (from variational principle) are written as: $\frac{d^2\varphi}{ds^2} = 0$. Meanwhile, at the free end, i.e., $s = a$, the classical moment (without strain gradient) would be zero which eventually gives; $\frac{d\varphi}{ds} = 0$. On the other hand, the moment (with strain gradient effect) would also be zero that further gives; $\frac{d\varphi}{ds} - l^2\frac{d^3\varphi}{ds^3} = 0$. In a nutshell, the boundary conditions considered in this work are written as:

$$\text{At } s = 0; \varphi = 0, \frac{d^2\varphi}{ds^2} = 0 \tag{18a}$$

$$\text{At } s = a; \frac{d\varphi}{ds} = 0, \frac{d\varphi}{ds} - l^2\frac{d^3\varphi}{ds^3} = 0 \text{ or } \frac{d\varphi}{ds} = 0, \frac{d^3\varphi}{ds^3} = 0 \tag{18b}$$

The nonlinear fourth-order differential equation (Eq. 17) with the respective boundary conditions (Eq. 18a) is solved using a three-stage Lobatto IIIa collocation formula. It is one of a widely used finite difference method to solve the boundary value problems. Details of this and some other relevant methods are provided by Shampine et al. [58].

3 Numerical results for the cantilever beam bending

For results, the material characteristic length (l) of epoxy, i.e., 17.6 μm [57] is taken to numerically evaluate the large deformation bending behavior of a cantilever beam. The concentrated vertical force F and height h are chosen in such a way that the beam remains elastic everywhere. In this study, the contribution of the surface residual stress toward the total surface stresses is found more noticeable than the surface elasticity, as shown by other researchers [33,50]. The end tip deflection for gradient model Y_g, non-gradient (large deformation) model Y_1 and the classical model Y_o ($FL^3/3EI$) are plotted in Fig. 2. It is shown that when $t_1 << h$, where t_1 is the ratio of the layer's thickness to the height of the beam, the effect of surface elasticity is negligible and all three models give similar results. Surface elasticity modulus is taken to be as: $E_s = E_1t_1$ and $E_1 = E = 1.44$ GPa [26,42]. The similar conclusion is drawn in the references [33,50]. Therefore, for further study, E_s and τ_o are assumed to be zero [59] and 0.2 μN/μm, respectively. The effect of the large deformation with increased load factor F_o ($F_o = Fa^2/2(EI)$) is shown by Joseph et al. [15], demonstrating its pronounced effect at the enhanced loads. The surface residual stress constant may be positive or negative [2]; therefore, results for both positive and negative residual stresses are presented. The vertical deflection of a cantilever beam along its axis, normalized with Y_o ($FL^3/3EI$) (classical endpoint vertical deflection), is presented in Fig. 3a. It can be seen, for smaller h/l ratios, that the gradient beam models are stiffer than the classical ones. The normalized deflections are shown to increase with increasing h/l, while the maximum deflection (at $s/a = 1$) of the strain gradient and classical model become comparable when $h/l \approx 1$ onwards. It is important to note that the effect of strain gradient is more prominent when $h/l \leq 0.2$; therefore, the subsequent results are primarily presented with $h/l \leq 0.2$. In Fig. 3b for $h/l \leq 0.2$, the results are obtained with strain gradient model with no surface effects, strain gradient model with positive surface residual stress and strain gradient model with negative surface residual stress. All effects have shown a significant contribution to the bending behavior of a cantilever beam. For instance, with the positive surface residual stress, the beam exhibits less stiff behavior and vice versa. This phenomenon is explained due to the sign of curvature associated with surface residual stress that causes an additional distributed load and change beam [26,51,59]. In the case of a positive surface residual stress, a positive curvature results in a positive distributed transverse force. This positive force increases the rotation of bending cantilever and thus beam behaves like a softer material. Meanwhile, this behavior is totally opposite when $\tau_o < 0$ and hence, the cantilever beam may exhibit a stiffer response comparatively.

The normalized maximum deflections (maximum tip deflection) for various beams configurations are numerically obtained using Eq. (6) and are shown in Fig. 4. Here, Y_g, Y_1 and Y_o ($Fa^3/(3EI)$) represent the deflection obtained with strain gradient model, non-gradient model and using the classical formulations (small deformation). Additionally, for comparison, the maximum tip deflections for positive and negative residual stresses are also included. The non-dimensional parameter ($\alpha = 3Fa^2/(Eh^4)$) as abscissa is defined for convenience. The normalized maximum deflection Y_g/Y_1 against α is plotted in Fig. 4a. From Fig. 4a, the strain gradient effect seems more pronounced for smaller (a/h), presenting smaller deflections and hence exhibiting stiffer response for the gradient beams. The effect of the surface residual stress on the tip deflections is shown to be more prominent for slender beams irrespective of h/l ratio. For a certain beam height, the effect of surface residual stress tends to increase with increasing beam length. Moreover, this behavior is also
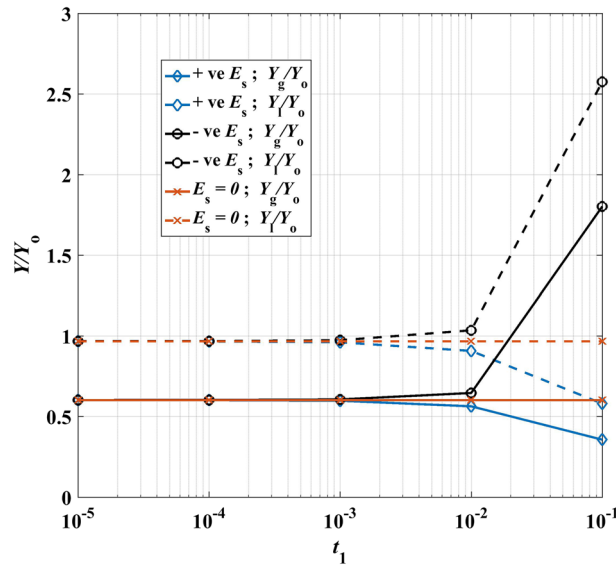
Fig. 2 Maximum tip deflection of the strain gradient model (Y_g) and the non-gradient model (Y_l), normalized with the classical results (Y_o) vs layer thickness to beam's height ratio ($t_1 = t/h$)

evident for increasing h/l ratio. It is clear that the positive surface residual stress induces larger tip transverse displacement while the opposite holds true for the negative surface residual stress. Figure 4b compares the strain gradient results with the classical model (without strain gradient & small deformation). It is shown for the smaller beam lengths that Y_g/Y_l and Y_g/Y_o are identical, indicating similar results for large as well as the small deformation theory. However, with an increase in beam slenderness (a/h ratio), the beam will undergo large deformation and hence the small deformation theory would over-estimate an endpoint vertical deflection. This is evident from a peak point (in each curve) in Fig. 4b, indicating classical model inadequacy to accurately predict the large deformation. Moreover, from Fig. 4b, it is quite evident that the pattern of maximum tip deflections, for the model with cumulative effects of strain gradient and surface residual stress, is similar to that of the model without surface residual stress (only strain gradient effect), apart from the fact that for positive surface residual stress the beam tends to exhibit softer behavior and vice versa. Nevertheless, from Fig. 4a, b, it may fairly be concluded that the effect of surface residual stress is more prominent for slender beams.

4 Fracture of a double cantilever beam with surface residual effect

Significant developments in the advance numerical methods have been made not only to accurately predict the fracture of various complex geometries [60,61] but also to cater the size effect on the fracture properties at smaller scale [6,7,62,63]. Adopting one of such numerical methods, in this section, the fracture property of a DCB, i.e., the stress intensity factor is evaluated numerically by taking the crack length to be the length of a beam as a and width b, the stress intensity factor (K) of a DCB may be written as $K = \sqrt{EG}$, where $G = F(dY_{max}/bda)$ and it is defined as the strain energy release rate of a DCB. Meanwhile, the classical result is given by $G_o = 12F^2a^2/(Eh^3b^2)$ (Wang & Wang, 2013). Figure 5 displays the normalized stress intensity factors versus α. For comparison, as in Fig. 4, the results for the strain gradient model K_g, non-gradient model K_l and classical theory K_o are given. Additionally, for further illustration, the stress intensity factors for the model with the positive and negative residual stresses are also included. Evidently, from Fig. 5, the effect of the surface residual stress is more prominent when $h/l \geq 0.075$ and for slender beams. It is clear that the positive residual stress enhances the stress intensity factors and vice versa. Furthermore, the effect of the negative surface residual stress is more noticeable as compared to the positive residual stress. For instance, in Fig. 5a, for $h/l \geq 0.1$ beyond certain peak point the normalized stress intensity factor shows a swift decline, signifying a stiffer beam response. However, this prompt observation is completely absent in the case of positive surface residual stress. Moreover, the normalizations of strain gradient results with the classical ones are shown in Fig. 5b. From Fig. 5b, apart from the strain gradient effects, it may clearly be seen that effect of negative
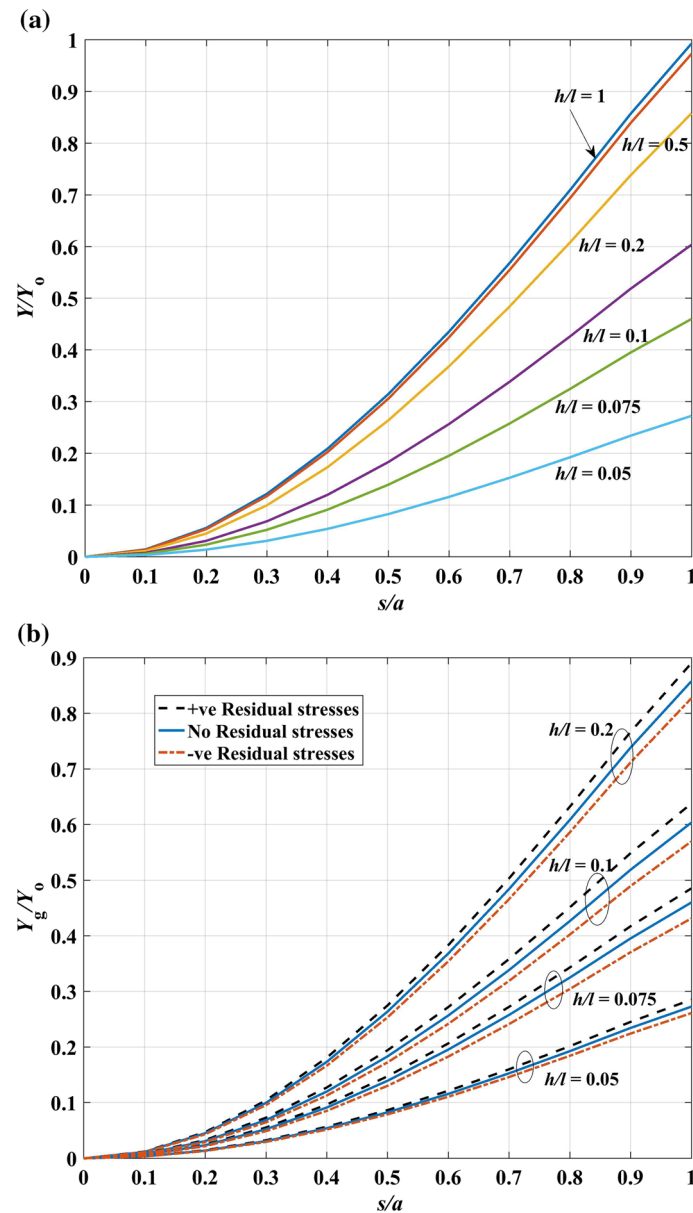
(a)

(b)

Fig. 3 a The vertical deflection along the beam axis (normalization with the classical result at the tip) for strain gradient models **b** The vertical deflection along the beam axis (normalization with the classical result at the tip) for the strain gradient models with surface residual effect

surface residual stress is more noticeable than that of the positive surface residual stress. On the other hand, the overestimation in the fracture characteristics is also evident following the trend as shown in Fig. 4.

5 Effect of the uncracked part

The strain gradient effect of the uncracked part of DCB is neglected (since strains in the uncracked part would be much lower than that in the cracked part). The schematic of uncracked part of a DCB is shown in Fig. 1b. The governing equation and respective boundary conditions of an uncracked part are provided by Wang & Wang [25] and Joseph et al. [15]. Here, it is necessary to mention the prominence of shear stresses at the uncracked part that must be incorporated in the constitutive equations. Therefore, Timoshenko beam model is more suitable to study the uncracked part of the DCB. Accordingly, the potential energy of an uncracked part
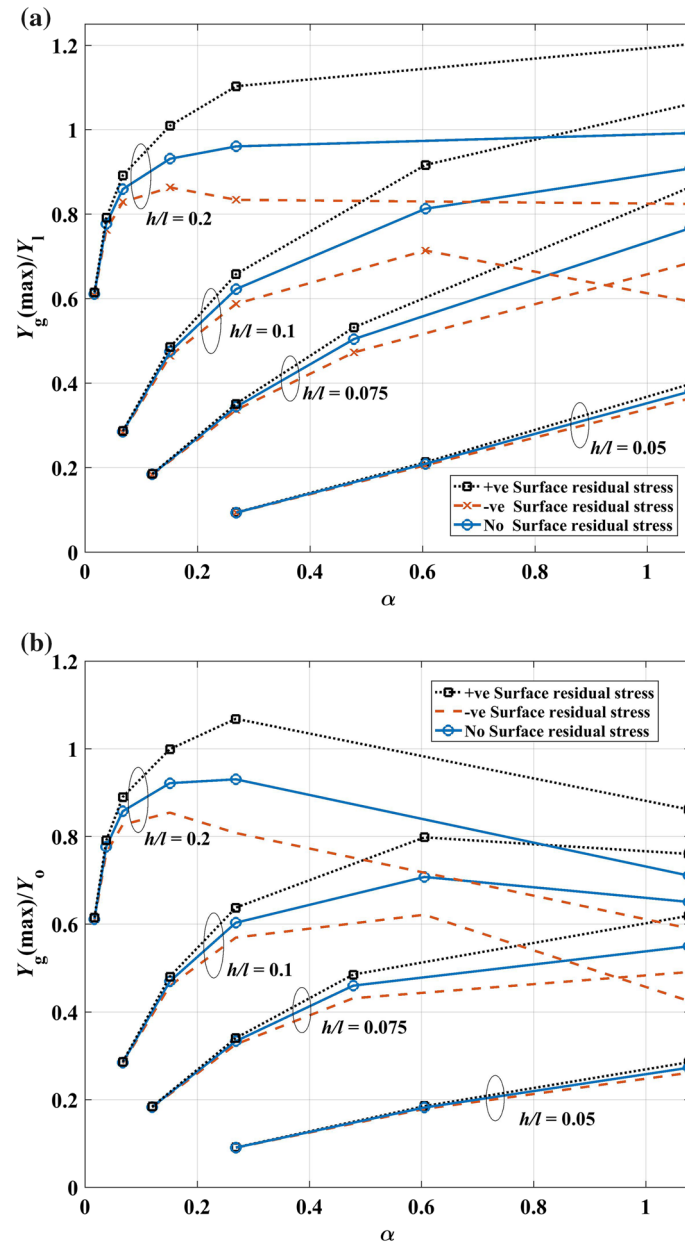
(a)

(b)

Fig. 4 **a** End point vertical deflection of the strain gradient model, normalization with the end point non-gradient vertical deflections (large deformation) **b** End point vertical deflection of the strain gradient model, normalization with the end point classical vertical deflections

(U_2) of DCB is given as:

$$U_2 = 2 \int\limits_{-\infty}^{0} \frac{M^2}{2EI_{\text{eff}}} \mathrm{d}x + 2 \int\limits_{-\infty}^{0} \frac{Q^2}{2G^s A} \mathrm{d}x \tag{19}$$

Here E is the Young's Modulus, G^s is the shear modulus, A is the area of cross-section and I_{eff} is the effective moment of inertia. Following the rectangular coordinate system, the integrals vary from negative
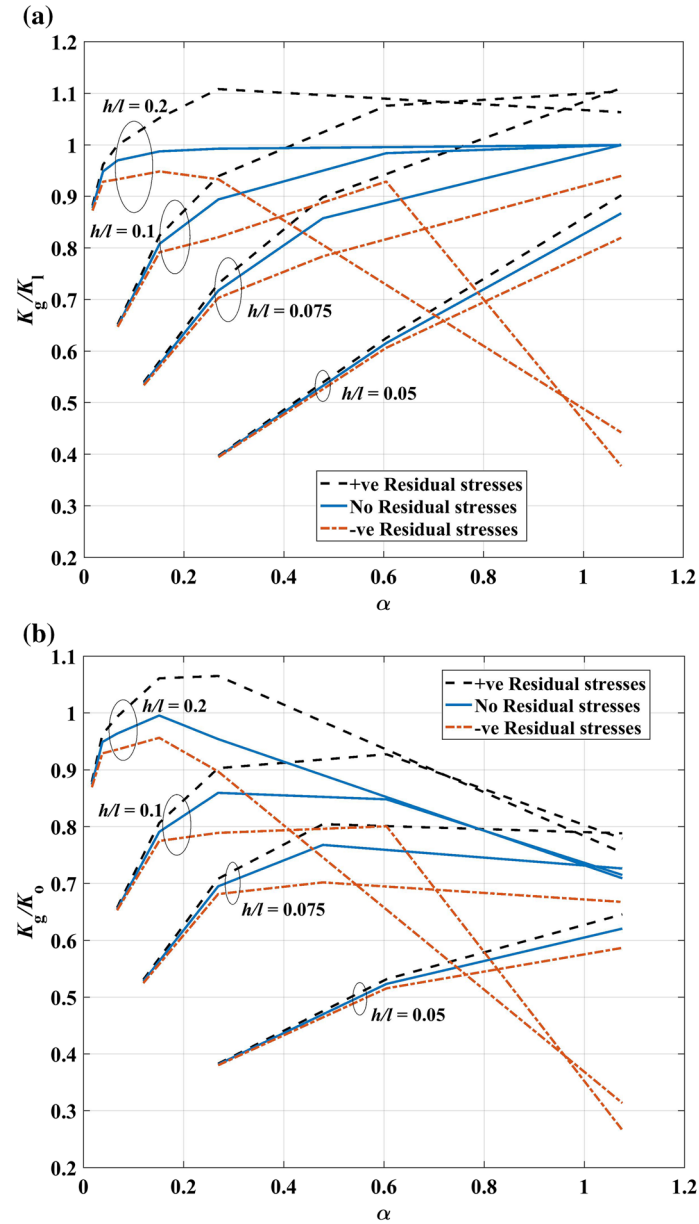
(a)

(b)

Fig. 5 a Stress intensity factors of the strain gradient model, normalization with the non-gradient stress intensity factors (large deformation) **b** Stress intensity factors of the strain gradient model, normalization with the classical stress intensity factors

infinity to zero. From the references [15,25] and using $M_{(\mathrm{o})} = F.X_{(\varphi_{\mathrm{o}})}$ we get:

$$U_2 = \frac{1}{\sqrt{EI_{\mathrm{eff}}GA}} \left[F^2 X_{(\varphi_{\mathrm{o}})}^2 + \left[\int_0^a sH\frac{\mathrm{d}\varphi}{\mathrm{d}s}\mathrm{d}s \right]^2 \right] \tag{20}$$

Now, the influence of the root part of DCB is investigated numerically. Here, R_{K} and R_{G} are defined, where R_{K} is the ratio of the stress intensity factor associated with the uncracked part to that of the cracked part of DCB, while R_{G} is the ratio of the strain energy release rate of an uncracked part to the cracked part. Variations of R_{K} and R_{G} versus a/h for different h/l ratios are plotted in Fig. 6. The results are plotted for strain gradient model without surface residual stress, strain gradient model with positive surface residual stress and strain gradient model with negative surface residual stress. It can be seen in Fig. 6 that, for a particular
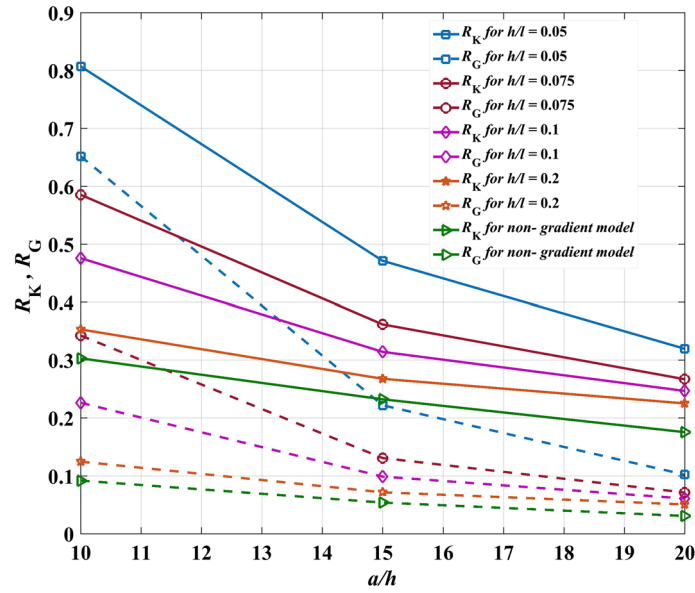
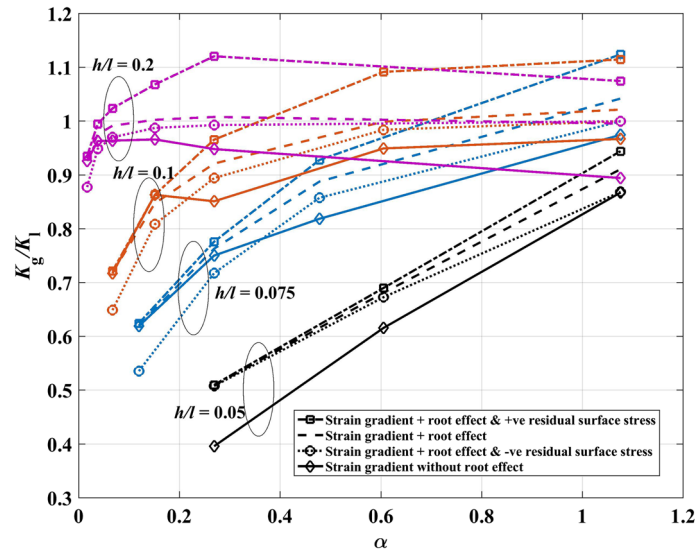**Fig. 6** Comparison of R_K and R_G plotted against a/h

Fig. 7 Stress intensity factors with the consideration of uncracked part of DCB, normalization with the non-gradient stress intensity factors (large deformation)

h/l, all models show the identical results. Thus, it may be stated that ratios R_K and R_G depend on the DCB geometry and it is independent of the surface residual stress. Moreover, it may equally be concluded that for smaller DCBs, i.e., for $h/l \leq 0.2$, the value of R_K and R_G may not be neglected even though the beam length to thickness ratio is higher ($a/h \approx 20$) (which was the case in classical studies).

The comparison of two strain gradient models, i.e., with root effect and without root effect in terms of stress intensity factors is shown in Fig. 7. The results are plotted for models incorporating strain gradient effect without surface residual stress, strain gradient effect with positive surface residual stress and strain gradient effect with negative surface residual stress. In general, results show that even with the incorporation of root effect, the positive surface residual stress causes DCB to exhibit softer response by enhancing the normalized stress intensity factor and vice versa. Again, this phenomenon may be explained due to the sign of curvature associated with negative surface residual stress that causes an additional distributed load (opposite to the direction of endpoint force), which in return cause the DCB to exhibit stiffer response. Hence, the influence

of the root effect of DCB must be considered in mathematical modeling for accurate prediction of its fracture properties. It seems true even for the slender beams ($a/h > 20$), lest an underestimated fracture behavior would be expected.

6 Conclusion

The cumulative effects of the strain gradient and surface stress on the large deformation bending behavior of a cantilever beam are investigated. Both surface elasticity and surface residual stress are incorporated in the mathematical modeling. Due to the negligible influence of surface elasticity, most of the results are depicted only with the consideration of surface residual stress. The results are obtained for the strain gradient model with no surface effects, strain gradient model with positive surface residual stress and negative surface residual stress individually. Due to the positive surface residual stress, the beam exhibits less stiff behavior. This softening behavior may be attributed to the sign of curvature that causes an additional distributed load and change beam stiffness. Meanwhile, this behavior is totally opposite in the case when $\tau_o < 0$; hence, a cantilever beam may exhibit a stiffer response comparatively. For the fracture property of DCB, i.e., stress intensity factor, the effect of the surface residual stress is shown to be increasing with increasing beam dimensions. In general, the influence of surface residual stress is more prominent when $h/l \geq 0.075$ and for slender beams. Moreover, the effect of negative surface residual stress was shown to be more noticeable than the positive surface residual stress. The root effect also enhances the normalized stress intensity factors. It was shown that the root effect on the ratios R_K and R_G for all three models remain same and thus it may be stated that R_K and R_G depend on the DCB geometry and are independent of the surface residual stress. It is observed for $h/l \leq 0.2$ that the significance of root effect must not be ignored.

References

1. Reeder, J.R., Crews Jr., J.: Nonlinear analysis and redesign of the mixed-mode bending delamination test (1991)
2. Wang, K., Wang, B.: Nonlinear fracture mechanics analysis of nano-scale piezoelectric double cantilever beam specimens with surface effect. Eur. J. Mech. A Solids **56**, 12–18 (2016)
3. Anderson, T., Nayfeh, A., Balachandran, B.: Experimental verification of the importance of the nonlinear curvature in the response of a cantilever beam. J. Vib. Acoust. **118**(1), 21–27 (1996)
4. Jia, X., Yang, J., Kitipornchai, S., Lim, C.W.: Free vibration of geometrically nonlinear micro-switches under electrostatic and Casimir forces. Smart Mater. Struct. **19**(11), 115028 (2010)
5. Jia, X.L., Yang, J., Kitipornchai, S.: Pull-in instability of geometrically nonlinear micro-switches under electrostatic and Casimir forces. Acta Mech. **218**(1–2), 161–174 (2011)
6. Giannakopoulos, A., Stamoulis, K.: Structural analysis of gradient elastic components. Int. J. Solids Struct. **44**(10), 3440–3451 (2007)
7. Stamoulis, K., Giannakopoulos, A.: A study of size effects and length scales in fracture and fatigue of metals by second gradient modelling. Fatigue Fract. Eng. Mater. Struct. **35**(9), 852–860 (2012)
8. Devitt, D., Schapery, R., Bradley, W.: A method for determining the mode I delamination fracture toughness of elastic and viscoelastic composite materials. J. Compos. Mater. **14**, 270–285 (1980)
9. Williams, J.: Large displacement and end block effects in the 'DCB' interlaminar test in modes I and II. J. Compos. Mater. **21**(4), 330–347 (1987)
10. Togun, N.: Nonlocal beam theory for nonlinear vibrations of a nanobeam resting on elastic foundation. Bound. Value Probl. **2016**(1), 1–14 (2016)
11. Wang, B., Hoffman, M., Yu, A.: Buckling analysis of embedded nanotubes using gradient continuum theory. Mech. Mater. **45**, 52–60 (2012)
12. Aifantis, E.C.: On the role of gradients in the localization of deformation and fracture. Int. J. Eng. Sci. **30**(10), 1279–1299 (1992)
13. Ru, C., Aifantis, E.: A simple approach to solve boundary-value problems in gradient elasticity. Acta Mech. **101**(1–4), 59–68 (1993)
14. Vardoulakis, I., Sulem, J.: Bifurcation Analysis in Geomechanics. Blackie Academic and Professional, Glasgow (1995)
15. Joseph, R.P., Wang, B., Samali, B.: Size effects on double cantilever beam fracture mechanics specimen based on strain gradient theory. Eng. Fract. Mech. **169**, 309–320 (2017)
16. Aifantis, E.C.: Update on a class of gradient theories. Mech. Mater. **35**(3), 259–280 (2003)
17. Aifantis, E.: Chapter one-internal length gradient (ILG) material mechanics across scales and disciplines. Adv. Appl. Math. **49**, 1–110 (2016)
18. Dingreville, R., Qu, J., Cherkaoui, M.: Surface free energy and its effect on the elastic behavior of nano-sized particles, wires and films. J. Mech. Phys. Solids **53**(8), 1827–1854 (2005)

19. Streitz, F., Cammarata, R., Sieradzki, K.: Surface-stress effects on elastic properties. I. Thin metal films. Phys. Rev. B **49**(15), 10699 (1994)
20. Fischer, F., Waitz, T., Vollath, D., Simha, N.: On the role of surface energy and surface stress in phase-transforming nanoparticles. Prog. Mater. Sci. **53**(3), 481–527 (2008)
21. Cahn, J.W.: Thermodynamics of Solid and Fluid Surfaces. In: Carter, W.C., Johnson, W.C. (eds.) The Selected Works of John W. Cahn, pp. 377–378. The Minerals, Metals & Materials Society, Pennsylvania (1998)
22. Cammarata, R.: Surface and interface stress effects on interfacial and nanostructured materials. Mater. Sci. Eng. A **237**(2), 180–184 (1997)
23. Cammarata, R.C.: Surface and interface stress effects in thin films. Prog. Surf. Sci. **46**(1), 1–38 (1994)
24. Fried, E., Gurtin, M.E.: The role of the configurational force balance in the nonequilibrium epitaxy of films. J. Mech. Phys. Solids **51**(3), 487–517 (2003)
25. Wang, B., Wang, K.: Effect of surface residual stress on the fracture of double cantilever beam fracture toughness specimen. J. Appl. Phys. **113**(15), 153502 (2013)
26. He, J., Lilley, C.M.: Surface effect on the elastic behavior of static bending nanowires. Nano Lett. **8**(7), 1798–1802 (2008)
27. Gurtin, M.E., Murdoch, A.I.: Surface stress in solids. Int. J. Solids Struct. **14**(6), 431–440 (1978)
28. Jammes, M., Mogilevskaya, S.G., Crouch, S.L.: Multiple circular nano-inhomogeneities and/or nano-pores in one of two joined isotropic elastic half-planes. Eng. Anal. Bound. Elem. **33**(2), 233–248 (2009)
29. Luo, J., Wang, X.: On the anti-plane shear of an elliptic nano inhomogeneity. Eur. J. Mech. A Solids **28**(5), 926–934 (2009)
30. Luo, J., Xiao, Z.: Analysis of a screw dislocation interacting with an elliptical nano inhomogeneity. Int. J. Eng. Sci. **47**(9), 883–893 (2009)
31. On, B.B., Altus, E., Tadmor, E.: Surface effects in non-uniform nanobeams: continuum vs. atomistic modeling. Int. J. Solids Struct. **47**(9), 1243–1252 (2010)
32. Wang, G.F., Feng, X.Q.: Effects of surface elasticity and residual surface tension on the natural frequency of microbeams. Appl. Phys. Lett. **90**(23), 231904 (2007)
33. Wang, G.F., Feng, X.Q.: Effect of surface stresses on the vibration and buckling of piezoelectric nanowires. Europhys. Lett. **91**(5), 56007 (2010)
34. Gurtin, M., Weissmüller, J., Larche, F.: A general theory of curved deformable interfaces in solids at equilibrium. Philos. Mag. A **78**(5), 1093–1109 (1998)
35. Shenoy, V.B.: Atomistic calculations of elastic properties of metallic fcc crystal surfaces. Phys. Rev. B **71**(9), 094104 (2005)
36. Weissmüller, J., Cahn, J.: Mean stresses in microstructures due to interface stresses: a generalization of a capillary equation for solids. Acta Mater. **45**(5), 1899–1906 (1997)
37. Duan, H., Wang, J., Huang, Z., Karihaloo, B.: Size-dependent effective elastic constants of solids containing nano-inhomogeneities with interface stress. J. Mech. Phys. Solids **53**(7), 1574–1596 (2005)
38. Sharma, P., Ganti, S.: Size-dependent Eshelby's tensor for embedded nano-inclusions incorporating surface/interface energies. J. Appl. Mech. **71**(5), 663–671 (2004)
39. Sharma, P., Ganti, S., Bhate, N.: Effect of surfaces on the size-dependent elastic state of nano-inhomogeneities. Appl. Phys. Lett. **82**(4), 535–537 (2003)
40. Chen, T., Chiu, M.S., Weng, C.N.: Derivation of the generalized Young–Laplace equation of curved interfaces in nanoscaled solids. J. Appl. Phys. **100**(7), 074308 (2006)
41. Ansari, R., Sahmani, S.: Bending behavior and buckling of nanobeams including surface stress effects corresponding to different beam theories. Int. J. Eng. Sci. **49**(11), 1244–1255 (2011)
42. He, J., Lilley, C.M.: Surface stress effect on bending resonance of nanowires with different boundary conditions. Appl. Phys. Lett. **93**(26), 263108 (2008)
43. Assadi, A., Farshi, B.: Vibration characteristics of circular nanoplates. J. Appl. Phys. **108**(7), 074312 (2010)
44. Assadi, A., Farshi, B., Alinia-Ziazi, A.: Size dependent dynamic analysis of nanoplates. J. Appl. Phys. **107**(12), 124310 (2010)
45. Zhang, L., Liu, J., Fang, X., Nie, G.: Size-dependent dispersion characteristics in piezoelectric nanoplates with surface effects. Physica E Low Dimens. Syst. Nanostruct. **57**, 169–174 (2014)
46. Fu, Y., Zhang, J.: Size-dependent pull-in phenomena in electrically actuated nanobeams incorporating surface energies. Appl. Math. Model. **35**(2), 941–951 (2011)
47. Koochi, A., Kazemi, A., Khandani, F., Abadyan, M.: Influence of surface effects on size-dependent instability of nano-actuators in the presence of quantum vacuum fluctuations. Phys. Scr. **85**(3), 035804 (2012)
48. Ma, J.B., Jiang, L., Asokanthan, S.F.: Influence of surface effects on the pull-in instability of NEMS electrostatic switches. Nanotechnology **21**(50), 505708 (2010)
49. Yang, F., Wang, G.F., Long, J.M., Wang, B.L.: Influence of surface energy on the pull-in instability of electrostatic nano-switches. J. Comput. Theor. Nanosci. **10**(5), 1273–1277 (2013)
50. Yan, Z., Jiang, L.: The vibrational and buckling behaviors of piezoelectric nanobeams with surface effects. Nanotechnology **22**(24), 245703 (2011)
51. Wang, K., Wang, B.: A general model for nano-cantilever switches with consideration of surface effects and nonlinear curvature. Physica E Low Dimens. Syst. Nanostruct. **66**, 197–208 (2015)
52. Aifantis, E.: Strain gradient interpretation of size effects. Int. J. Fract. **95**(1–4), 299–314 (1999)
53. Askes, H., Suiker, A., Sluys, L.: A classification of higher-order strain-gradient models-linear analysis. Arch. Appl. Mech. **72**(2–3), 171–188 (2002)
54. Christensen, J., Bastien, C.: Nonlinear Optimization of Vehicle Safety Structures: Modeling of Structures Subjected to Large Deformations. Butterworth–Heinemann, Oxford (2015)
55. Wang, G.F., Feng, X.Q.: Surface effects on buckling of nanowires under uniaxial compression. Appl. Phys. Lett. **94**(14), 141913 (2009)
56. Kahrobaiyan, M., Rahaeifard, M., Tajalli, S., Ahmadian, M.: A strain gradient functionally graded Euler–Bernoulli beam formulation. Int. J. Eng. Sci. **52**, 65–76 (2012)

57. Kong, S., Zhou, S., Nie, Z., Wang, K.: Static and dynamic analysis of micro beams based on strain gradient elasticity theory. Int. J. Eng. Sci. **47**(4), 487–498 (2009)
58. Shampine, L.F., Kierzenka, J., Reichelt, M.W.: Solving boundary value problems for ordinary differential equations in MATLAB with bvp4c. Tutorial notes (2000)
59. Wu, Q., Volinsky, A.A., Qiao, L., Su, Y.: Surface effects on static bending of nanowires based on non-local elasticity theory. Prog. Nat. Sci. Mater. Int. **25**(5), 520–524 (2015)
60. Fleming, M., Chu, Y., Moran, B., Belytschko, T., Lu, Y., Gu, L.: Enriched element-free Galerkin methods for crack tip fields. Int. J. Numer. Methods Eng. **40**(8), 1483–1504 (1997)
61. Joseph, R., Purbolaksono, J., Liew, H., Ramesh, S., Hamdi, M.: Stress intensity factors of a corner crack emanating from a pinhole of a solid cylinder. Eng. Fract. Mech. **128**, 1–7 (2014)
62. Guha, S., Sangal, S., Basu, S.: Finite element studies on indentation size effect using a higher order strain gradient theory. Int. J. Solids Struct. **50**(6), 863–875 (2013)
63. Joseph, R.P., Wang, B., Samali, B.: Strain gradient fracture in an anti-plane cracked material layer. Int. J. Solids Struct.(2018, in press)